Available online at www.sciencedirect.com
ScienceDirect
Journal of Solid State Chemistry 180 (2007) 2550–2557
JOURNAL OF SOLID STATE CHEMISTRY
www.elsevier.com/locate/jssc

Structure and properties of the $CaFe_2O_4$-type cobalt oxide $CaCo_2O_4$

Mitsuyuki Shizuya, Masaaki Isobe*, Eiji Takayama-Muromachi

Advanced Nano Materials Laboratory, National Institute for Materials Science (NIMS), 1-1 Namiki, Tsukuba, Ibaraki 305-0044, Japan

Received 31 May 2007; received in revised form 13 July 2007; accepted 15 July 2007
Available online 21 July 2007

Abstract

The calcium cobalt oxide $CaCo_2O_4$ was synthesized for the first time and characterized from a powder X-ray diffraction study, measuring magnetic susceptibility, specific heat, electrical resistivity, and thermoelectric power. $CaCo_2O_4$ crystallizes in the $CaFe_2O_4$ (calcium ferrite)-type structure, consisting of an edge- and corner-shared CoO_6 octahedral network. The structure of $CaCo_2O_4$ belongs to an orthorhombic system (space group: *Pnma*) with lattice parameters, $a = 8.789(2)$ Å, $b = 2.9006(7)$ Å and $c = 10.282(3)$ Å. Curie–Weiss-like behavior in magnetic susceptibility with the nearly trivalent cobalt low-spin state (Co^{3+}, $3d\ t_{2g}^6$, $S = 0$), semiconductor-like temperature dependence of resistivity ($\rho = 3 \times 10^{-1}\,\Omega$cm at 380 K) with dominant hopping conduction at low temperature, metallic-temperature-dependent large thermoelectric power (Seebeck coefficient: $S = +147\,\mu$V/K at 380 K), and Schottky-type specific heat with a small Sommerfeld constant ($\gamma = 4.48(7)$ mJ/Co mol K^2), were observed. These results suggest that the compound possesses a metallic electronic state with a small density of states at the Fermi level. The doped holes are localized at low temperatures due to disorder in the crystal. The carriers probably originate from slight off-stoichiometry of the phase. It was also found that S tends to increase even more beyond 380 K. The large S is possibly attributed to residual spin entropy and orbital degeneracy coupled with charges by strong electron correlation in the cobalt oxides.

Keywords: Cobalt oxide; $CaFe_2O_4$-type structure; High-pressure synthesis; Thermoelectric power

1. Introduction

In the past several years, extensive studies have been carried out on the solid-state physics and chemistry of cobalt oxides because these materials possess strong electronic correlation and thus, exhibit unusual properties. Researchers have usually looked at the unconventional superconductivity observed below 5 K in hydrated $Na_{0.35}CoO_2 \cdot 1.3H_2O$ [1]. This superconductivity is quite interesting because of the unconventional Cooper pairing, possibly mediated by the magnetic fluctuations [2]. Furthermore, interest has grown in the large thermoelectric power coexisting with low electric resistivity in layered cobalt oxides, such as $NaCo_2O_4$ [3] and $Ca_3Co_4O_9$ [4]. This effect is considered to be attributed to the large residual entropy associated with spin frustration on the triangle lattice in the CoO_2 layer [5]. Lately, the search for new materials and the precise characterization of the materials have intensified, in order to further improve the understanding of the unusual physical properties and, ultimately, the essence of the electron correlation in transition-metal oxides.

In contrast, the $CaFe_2O_4$ (calcium ferrite)-type structure is very intriguing for solid-state chemists [6]. The prototype $CaFe_2O_4$ crystallizes in an orthorhombic structure with lattice constants $a = 9.217$ Å, $b = 10.702$ Å, and $c = 3.018$ Å (space group: *Pnam*), built of eight-fold-coordinated Ca atoms and distorted FeO_6 octahedra [7]. It has been reported that the Ca and Fe atoms can be independently replaced with different elements and resulting in the same crystallization structure. So far, a variety of related compounds having the $CaFe_2O_4$-type structure have been found. For instance, AB_2O_4 (A = Li, Na, Mg, Ca, Sr, Ba, La, and Eu; B = Ti, V, Cr, Mn, Fe, Ru, Rh, Al, Ga, In, Tl, Sc, Y, La, Pr, Nd, Sm, Eu, Gd, Tb, Dy, Ho, Yb, and Lu) have been reported [8–18]. Although many 3*d* elements can be substituted at the Fe site

*Corresponding author. Fax: +81 29 860 4674.
E-mail address: ISOBE.Masaaki@nims.go.jp (M. Isobe).

0022-4596/$ - see front matter © 2007 Elsevier Inc. All rights reserved.
doi:10.1016/j.jssc.2007.07.008

in $CaFe_2O_4$, the substitution of the Co, Ni and Cu elements with other elements has not been reported, to the best of the authors' knowledge.

The $CaFe_2O_4$-type structure includes edge- and corner-sharing BO_6 octahedra, constituting a very distinctive network similar to the one formed in perovskite-related compounds. This structural network suggests that interesting physical properties may exist in the $CaFe_2O_4$-type compounds, where the *B*-site atoms are transition-metal magnetic elements, such as high-T_C superconductivity in cuprates [19], quantum magnetic characters in ruthenates [20], strongly correlated features in manganates [21], etc. In particular, unique quantum behavior characteristic of low-dimensional systems may occur in the $CaFe_2O_4$-type compounds. This is because the edge-sharing connection of the octahedra forms a double-chain structure, which can be regarded as a part of the CdI_2-type structure observed in the layered cobalt oxides [3,4]. Thus, the t_{2g} orbital configuration of the *B*-site atoms in the double chain is expected to orientate towards neighboring *B*-site atoms and overlap, suggesting that the direct charge transfer through the t_{2g} orbitals may cause stronger intra-chain magnetic interaction between the *B*-site spins than inter-chain interaction.

Motivated by this hypothesis, we have searched for a new phase of the $CaFe_2O_4$-type group which has an active BO_6 network in a magnetic and electrical sense. As a result of the experiments of the new-phase search, we recently succeeded in synthesizing a new $CaFe_2O_4$-type cobalt oxide, $CaCo_2O_4$, using solid-state reaction at a condition of high temperature and high pressure. It was found that the cobalt valence of the calcium cobaltite is near to the 3+ low-spin state with a $3d$ t_{2g}-orbital electric band almost filled with electrons (Co^{3+}, $3d$ t_{2g}^6, $S=0$).

In this paper, we report on the synthesis, crystal structure and the magnetic and electrical transport properties of the new cobaltite, $CaCo_2O_4$. In particular, we emphasize that this novel compound can exhibit large thermoelectric power and unusual temperature dependence of the Seebeck coefficient. We discuss the electronic state of the system and origin of the unusual properties in terms of residual spin entropy and orbital degeneracy in the t_{2g} orbital.

2. Experimental

Polycrystalline samples of $CaCo_2O_4$ were prepared from a solid-state reaction using a high-pressure synthesis technique. Starting reagents, Co_3O_4 (3 N) and $(Ca_2CoO_3)_{0.62}CoO_2$ [22], were mixed in an agate mortar with a molar ratio of '0.86:3', respectively. The mixture was dried in flowing O_2 gas at 300 °C for several hours, and then placed into platinum capsules (6.8 mm in diameter, 0.2 mm in thickness, and approximately 5 mm in height) in a globe box filled with dry Ar gas. Previous to the preparation, the $(Ca_2CoO_3)_{0.62}CoO_2$ powder had been prepared from Co_3O_4 and $CaCO_3$ (3 N) by heating in O_2 at 900–950 °C for several days with intermediate grindings. The platinum capsules were heated at 1500 °C for 1 h under 6 GPa using a flat-belt-type high-pressure apparatus, and then quenched to room temperature before the pressure was released. The sintered samples were dense, black, and retained a pellet shape. The surfaces of the pellets were carefully scraped to remove any possible contaminations from chemical reactions with the platinum capsule. The typical sample weight was ~0.4 g.

Phase purity and crystal structure of the products were studied using conventional powder X-ray diffraction (XRD). The XRD patterns were obtained using Cu$K\alpha$ radiation from a diffractometer (Rigaku, RINT-ULTIMA III) equipped with Bragg–Brentano geometry with a goniometer radius of 285 mm and a conventional slit system. The crystal structure was analyzed using the X-ray Rietveld method with the software RIETAN-2000 [23]. The intensity data for the refinement were collected at room temperature in a 2θ angle range of 10–110° using a step-scan (fixed-time) mode with a 2θ step size of 0.02° and a data-collection time of 30 s per step. The slit condition was set as follows: divergence-slit width = scattering-slit width = 1/3° and receiving-slit width = 0.3 mm. Interatomic distances and bond-angles were calculated from the refined positional parameters using a computer program ORFFE [23].

The Seebeck coefficient was measured between 10 and 390 K with a four-probe configuration, using a thermal transport option (TTO) in a commercial apparatus (Quantum Design, PPMS). The sample size was $1.5\times2.1\times5.5\,mm^3$, and the distance between temperature/voltage terminals was 2.9 mm. Fine copper wires (cross section: $\sim0.24\times0.64\,mm^2$) were attached onto the polished sample surface via an evaporated gold film using silver paste, in order to make a good ohmic contact. Data were collected using the continuous mode at a cooling rate of 0.3 K/min. Temperatures at the terminals were obtained from thermometers (Cernox 1050), and the temperature difference between the terminals was kept to within 3% of the measurement temperature. The electrical resistivity was measured using the conventional four-probe ac method simultaneously with the Seebeck coefficient measurement. The ac current of 0.01–0.05 mA at 60–300 Hz was applied to the sample.

The magnetic susceptibility was measured on a pulverized sample (200.97 mg) using a superconducting-quantum-interference-device (SQUID) magnetometer (Quantum Design, MPMS-XL) at a magnetic field of 1 kOe between 5 and 350 K on heating and cooling. The specific heat measurement was performed using a bulk specimen (12.34 mg) in the PPMS system with a time-relaxation method over the temperature range 2–300 K.

3. Results and discussion

Fig. 1 is the powder X-ray diffraction pattern of $CaCo_2O_4$. All the Bragg reflections can be systematically indexed with an orthorhombic system with lattice parameters,

$a = 8.789(2)$ Å, $b = 2.9006(7)$ Å and $c = 10.282(3)$ Å. It indicates that the sample is of high quality; there is no significant impurity in the product. Extinctions of the reflections are $k+l=2n$ for $0kl$ and $h=2n$ for $hk0$. Possible space groups are, therefore, presumed to be *Pnma* (No. 62) and $Pn2_1a$ (No. 33). In this paper, we assume that the higher symmetry, *Pnma*, is a suitable space group of $CaCo_2O_4$, where this space group is the same as $CaFe_2O_4$ [6,7].

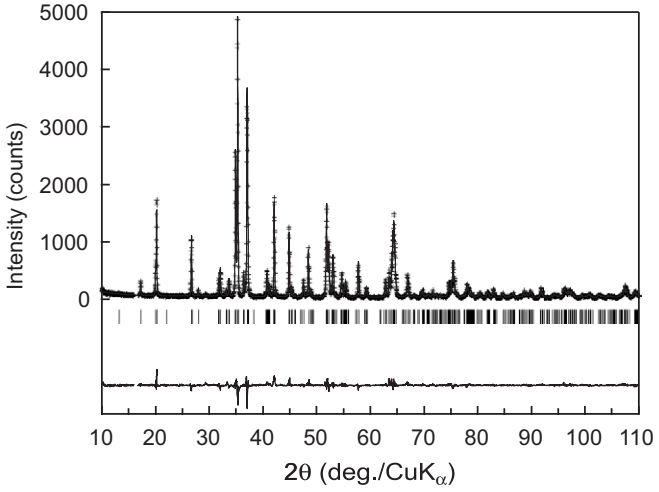

Fig. 1. Powder X-ray diffraction pattern of $CaCo_2O_4$ for the Rietveld analysis. The observed and calculated patterns are indicated by crosses and a solid line, respectively. The difference between the observed pattern and the calculated one is presented at the bottom of the figure. Tick marks indicate positions of allowed Bragg reflections. A small extra reflection at $2\theta = 16.5^\circ$ was purposely excluded from the data to improve the reliability factors.

The crystal structure of $CaCo_2O_4$ was studied using the X-ray Rietveld analysis method. Atomic coordinates and thermal displacement parameters for all the sites were refined with the RIETAN-2000 program. The structure parameters of $CaFe_2O_4$ were employed as an initial model in the refinement. The best refinement result, i.e., the X-ray Rietveld profile, is shown in Fig. 1. The difference curve (bottom part of the figure) clearly indicates that the observed X-ray profile can be precisely reproduced from the profile calculated using the similar structure model as $CaFe_2O_4$. The structure parameters and crystallographic data of $CaCo_2O_4$ are summarized in Table 1, whereas the selected bond distances and angles are in Table 2.

Fig. 2(a) is a schematic view of the crystal structure of $CaCo_2O_4$, illustrated using the parameters from Table 1. The structure is essentially identical to that of the prototype compound, $CaFe_2O_4$. The most characteristic feature in the structure of $CaCo_2O_4$ is the double Co–O

Table 2
Selected bond distances (Å) and angles (°) of $CaCo_2O_4$

Co_1–O_1		1.973(7)	Co_2–O_1	× 2	1.982(4)
Co_1–O_2	× 2	1.940(4)	Co_2–O_3		1.977(6)
Co_1–O_2		1.885(6)	Co_2–O_4	× 2	1.942(4)
Co_1–O_3	× 2	1.920(4)	Co_2–O_4		1.914(5)
Co_1–O_2–Co_1[a]		96.7(2)	Co_1–O_1–Co_2		123.0(2)
Co_1–O_2–Co_1[b]		98.0(2)	Co_1–O_3–Co_2		130.9(1)
Co_1–O_3–Co_1		98.1(2)			
Co_2–O_1–Co_2		94.0(2)			
Co_2–O_4–Co_2[a]		96.6(2)			
Co_2–O_4–Co_2[b]		97.0(2)			

[a]Atom in the same chain; symmetry operator: x, $y+1$, z (Co_1, Co_2).
[b]Atom in the neighboring chain; symmetry operator: $-x+1$, $y+1/2$, $-z$ (Co_1), $-x+1$, $y+1/2$, $-z+1$ (Co_2).

Table 1
Atomic coordinates, isotropic displacement parameters, and crystallographic data of $CaCo_2O_4$

Atom	Site	g[a]	x	y	z	B (Å^2)
Ca	4*c*	1	0.7619(3)	1/4	0.6644(2)	0.70(6)
Co_1	4*c*	1	0.4160(2)	1/4	0.0980(2)	0.25(4)
Co_2	4*c*	1	0.4431(2)	1/4	0.6114(1)	0.25[b]
O_1	4*c*	1	0.2018(7)	1/4	0.1552(6)	1.0[a]
O_2	4*c*	1	0.1127(7)	1/4	0.4751(6)	1.0[a]
O_3	4*c*	1	0.5259(9)	1/4	0.7902(6)	1.0[a]
O_4	4*c*	1	0.4168(7)	1/4	0.4266(5)	1.0[a]

Formula	$CaCo_2O_4$
Molecular weight	221.942
Temperature	r.t.
Wavelength	1.540593 Å (Cu$K\alpha$)
Space group	*Pnma* (No. 62)
Lattice constants	$a = 8.789(2)$ Å, $b = 2.9006(7)$ Å, $c = 10.282(3)$ Å, $V = 262.1(1)$ Å^3
Z	4
Density (calculated)	5.624 g/cm^3
R-factors	$R_{wp} = 0.1200$, $R_p = 0.0897$, $R_B = 0.0488$, $R_F = 0.0242$, $S = R_{wp}/R_e = 1.3588$
Refinement Software	RIETAN-2000

[a]Fixed in the refinement.
[b]The thermal parameters of Co atoms were grouped and refined together: constraint on $B(Co_1) = B(Co_2)$.

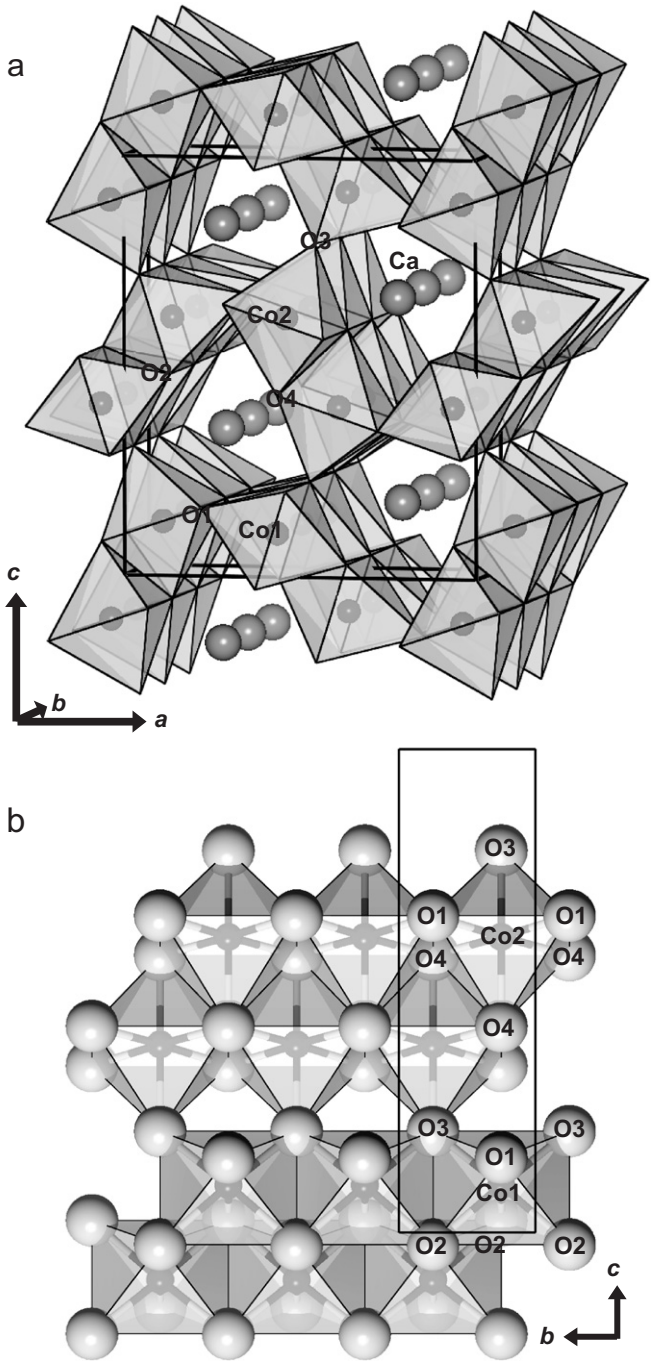

Fig. 2. A representation (a) of the crystal structure of $CaCo_2O_4$, where the bold lines show the orthorhombic unit cell, (b) is the CoO_6-octahedra network, projected along the a-axis ($0.2 \leqslant x \leqslant 0.8$). The double chains run along the b-axis.

chain, running along the b-axis, as is sketched out in Fig. 2(b). The CoO_6 octahedra are connected by edge sharing within each double chain. The double chains are tied to neighbors by corner oxygen sharing. The double chain includes a part of the triangle lattice of a Co-atom network, indicating that the cobalt t_{2g} orbital is orientated towards neighboring Co-atoms and the orbitals probably overlap between the atoms within the double chain.

The Co–O inter-atomic distances in the CoO_6 octahedron are 1.89–1.97 Å for the Co_1–O bonds and 1.91–1.98 Å for the Co_2–O bonds. The average distance, 1.943 Å, is consistently near to the value 1.945 Å, estimated from the summation of the effective ionic radii of Co and O:0.545 Å for Co^{3+} (six-fold coordination with a low-spin state) and 1.40 Å for O^{2-} (six-fold coordination) [24]. The Co_1–O_2 bond (1.89 Å) (or the Co_2–O_4 bond (1.91 Å)) is shorter than the Co_1–O_1 bond (1.97 Å) (or the Co_2–O_3 bond (1.98 Å)), indicating that the Co atom is somewhat unevenly situated toward the inside of the double chain within the cage of the octahedron. The intra-chain Co–O–Co bond angle is $\sim 96 \pm 2^\circ$ (average of the Co_1–O_2(or O_3)–Co_1 and Co_2–O_4(or O_1)–Co_2 bond angles). In contrast, the inter-chain Co–O–Co bond angle is approximately 123° for Co_1–O_1–Co_2 and 131° for Co_1–O_3–Co_2. The inter-chain bond connectivity is expected to influence the dimensionality of the electrical conductivity. In particular, the inter-chain Co–O–Co bond-angle would affect the dimensionality more than the bond distances. The observed deviation of the inter-chain Co–O–Co angle from 180° suggests possible overlap in part of the cobalt t_{2g} orbitals between the chains. It may cause deviation from the one-dimensional (1-D) anisotropy of the electronic conducting state. Actually, 3-D (or 2-D)-like carrier conduction and magnetic behavior were observed in $CaCo_2O_4$, as is shown later.

Fig. 3 is a plot of the magnetic susceptibility χ of $CaCo_2O_4$ as a function of temperature. Neither magnetic transition nor low-dimensional behavior was observed. The temperature (T) dependence is similar to the Curie–Weiss law. The susceptibility data in the temperature range $5\,\mathrm{K} \leqslant T \leqslant 350\,\mathrm{K}$ were numerically fitted with the conventional formula, $\chi = \chi_0 + C/(T-\theta_W)$, where χ_0 is a temperature-independent component of the susceptibility, C is a Curie constant, and θ_W is a Weiss temperature. As a result of the

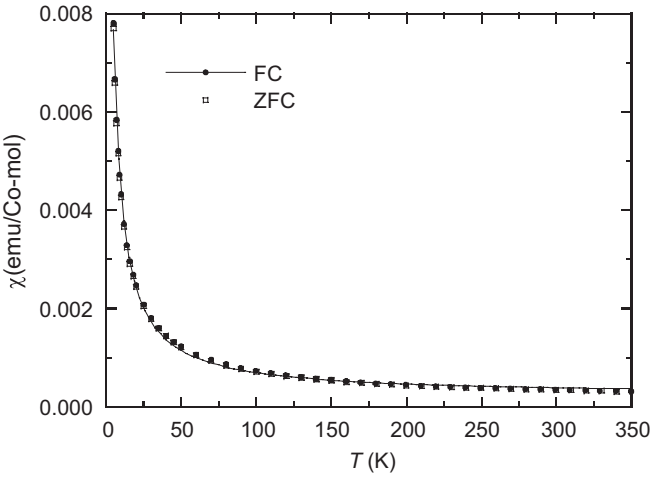

Fig. 3. Temperature dependence of the magnetic susceptibility χ per cobalt ion for $CaCo_2O_4$. The solid curve represents Curie–Weiss-law approximation between 5 and 350 K; $\chi = \chi_0 + C/(T-\theta_W)$: $\chi_0 = 2.2(1) \times 10^{-4}$ emu/Co mol, $C = 0.0471(6)$ emu K/Co mol, and $\theta_W = -1.3(1)$ K.

curve-fit analysis, the following parameters were obtained, $\chi_0 = 2.2(1) \times 10^{-4}$ emu/Co mol, $C = 0.0471(6)$ emu K/Co mol, and $\theta_W = 1.3(1)$ K. The χ_0 component is comprised of a diamagnetic term of the closed inner shell of the atoms, a Van Vleck paramagnetic term of the orbitals, and, if any, a Pauli paramagnetic term of the carriers. The small C value could be understood that minority spins are mixed with a dominant cobalt 3+ low-spin non-magnetic state (Co^{3+}, $3d\ t_{2g}^6$, $S = 0$). The number of spins corresponds to maximum ~12% of all the Co ions, if all the active spins are of $S = 1/2$. (It is ~1.5% if $S = 2$.) The active spins probably originate from complex factors: impurities, lattice imperfections, localized net carriers produced by slight off-stoichiometry of the phase, etc. It should be noted that the localized carriers contribute to a part of the magnetic signal. Presence of the small number of carriers is supported by the transport properties and specific heat measurements, as shown later. The small θ_W value is indicative of a weak inter-spin correlation. The results suggest that the magnetic signal of $CaCo_2O_4$ is principally due to the localized dilute spins with a weak magnetic interaction.

Fig. 4 is a plot of the electrical resistivity ρ of a polycrystalline $CaCo_2O_4$ as a function of temperature. The semiconductor-like temperature dependence of the resistivity was observed over the whole measured temperature range. The absolute value is $\sim 3 \times 10^{-1}\,\Omega$cm at 380 K, a typical value for electrically conductive transition-metal oxides having an intermediate electronic state between gap semiconductors and metals. The resistivity value increases over several magnitudes for a decreasing temperature. The curvature of the ρ–T plot between 100 and 250 K changes slowly. Within the same temperature range, it was also found that the Seebeck coefficient S of $CaCo_2O_4$ changes with temperature, as is shown later.

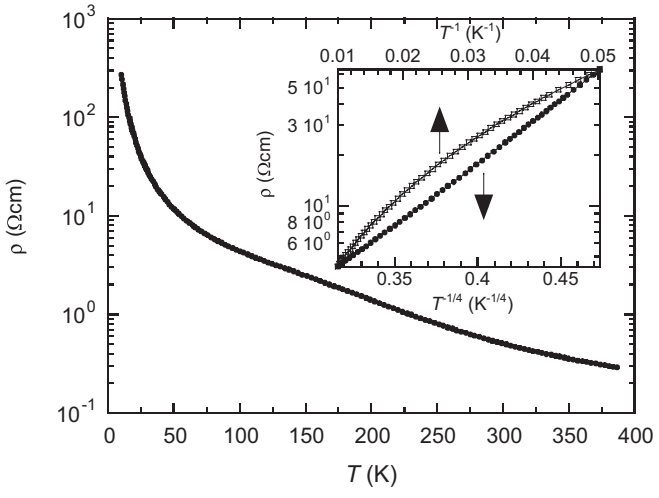

Fig. 4. Temperature dependence of the electrical resistivity ρ for a polycrystalline sample of $CaCo_2O_4$. Inset: Arrhenius ($\ln\rho$ vs. $1/T$) and Mott variable-range hopping ($\ln\rho$ vs. $1/T^{0.25}$) plots, for comparison of the two mechanisms of low-temperature carrier conduction.

The semiconducting behavior observed from the resistivity measurements seems to be consistent with the simple expectation that the cobalt t_{2g} band should almost be filled with electrons. To see more precise features of the electronic state near the Fermi level (E_F), the resistivity data between 20 and 100 K were plotted in two independent formats, logarithmic ρ vs. $1/T$ (Arrhenius) and $1/T^{0.25}$ (variable-range hopping: VRH [25–27]), as shown in the inset in Fig. 4. The data show nearly linear behavior in the latter form, suggesting a hopping conduction mechanism is dominant in $CaCo_2O_4$. It implies that a small number of carriers are localized at low temperature, probably due to the disorder in the crystal. Presumably, the Fermi level barely crosses the near-edge of the t_{2g} band or an in-gap state, forming a small density of states at E_F. The shift of E_F is probably due to slight off-stoichiometry of the phase. The dopant feature can be seen also in the properties of the Seebeck coefficient and specific heat of $CaCo_2O_4$, as shown later.

Near room temperature ($\gtrsim \theta_D/2$; θ_D: Debye temperature), the resistivity response is similar to a thermal-activation type rather than the VRH type [28]. It implies that the dominant conduction mechanism may vary from the VRH type to another type when the temperature is increased. There are several possible mechanisms explaining the thermal-activation-type resistivity behavior: e.g., carrier excitation from E_F to a mobility edge (E_c) of the band ($\rho(T) \propto \exp((E_c - E_F)/k_BT)$ [25–27]), small polaron ($\rho(T) \propto T^{3/2}\exp((E_c - E_F + W_H)/k_BT)$; W_H: hopping energy, non-adiabatic expression [25–27,29]), grain-boundary scattering ($\rho(T) \propto T^{1/2}\exp(E_B/k_BT)$; E_B: barrier potential, thermal-ion emission type [30,31]), etc. The broad hump observed for $100\,K \leqslant T \leqslant 250\,K$ might be due to a kind of transitional process or thermal crossover from the VRH conduction to a different mechanism that operates in the excited state. In any case, more precise studies using a single-crystal sample are necessary to provide conclusive evidence of a dominant mechanism. The accurate carrier density and mobility measurements, both parallel and perpendicular to the chain direction (the b-axis), would be required.

Fig. 5 is a plot of the Seebeck coefficient S of $CaCo_2O_4$ as a function of temperature. The S is positive over the whole measured temperature range, indicating that transport is dominated by p-type carriers. There are three distinct regions in the data plotted in Fig. 5: (1) S increases linearly for $20\,K \leqslant T \leqslant 100\,K$, (2) a decrease in the slope is observed for $100\,K \leqslant T \leqslant 250\,K$, and (3) the slope then increases for temperatures above 250 K. The observed increase in S can be explained as part of the metallic behavior of the material in this temperature range. The electronic state of $CaCo_2O_4$ is metallic, and a finite density of states exists at E_F. The low-temperature ($20\,K \leqslant T \leqslant 100\,K$) data were analyzed with a variable-range hopping (VRH) scheme [25–27]. The inset in Fig. 5 is a plot of $\ln S$ as a function of $\ln T$. The slope of this plot corresponds to the dimensionality of the hopping

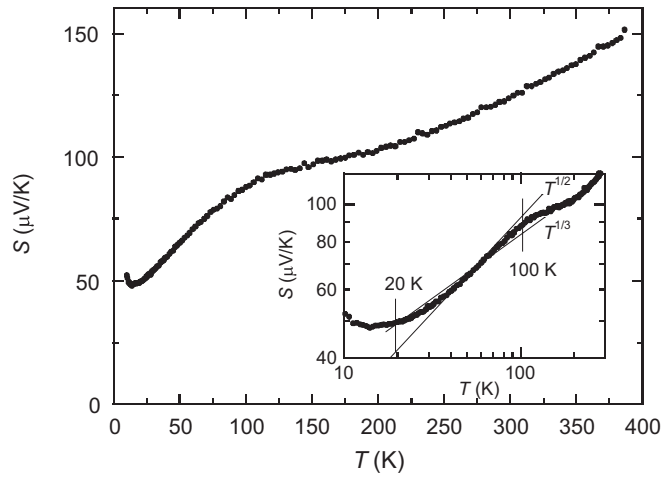

Fig. 5. Temperature dependence of the Seebeck coefficient S for $CaCo_2O_4$. Inset: Logarithm plot, $\ln S$ vs. $\ln T$, for comparison between the dimensionalities of low-temperature carrier conduction.

conduction. The results confirm the dominant 3-D ($S \propto T^{1/2}$) or 2-D ($S \propto T^{1/3}$) VRH regime in the ground state. At least, a 1-D case ($S \propto T^{-1}$) is most unlikely [32]. The 3-D (or 2-D) character of S may reflect the charge transfer between the neighboring chains, i.e., the inter-chain orbital hybridization of the cobalt atoms. This result is consistent with the 3-D (or 2-D)-like structural features, as seen in the inter-chain Co–O–Co bond angles.

We found an anomaly in the temperature gradient of S at ~100 K. This phenomenon appeared in the process of the transition from the VRH regime in the ground state to another regime of a thermally excited state; however, this other regime has not yet been identified. The changes in the slope of S correlate with the change of the curvature observed in the resistivity data (Fig. 4). This implies that the two physical parameters, S and ρ, correlate to each other in $CaCo_2O_4$. For usual metals S at a certain temperature can be expressed as

$$S = \left(\frac{\pi^2}{3}\right)\left(\frac{k_B^2 T}{e}\right)\left(\frac{d \ln \sigma}{dE}\right)_{E=E_F}, \quad (1)$$

where k_B, e, and σ are the Boltzmann constant, unit charge of an electron, and conductivity, respectively [25–27]. This equation indicates a relationship between the differential conductivity and Seebeck coefficient. The change in the slope of S may suggest a significant modification of the electronic structure near the Fermi level, around 100 K.

$CaCo_2O_4$ exhibits large Seebeck coefficient above room temperature. The typical absolute value of S is ~147 μV/K at 380 K. This value is larger than those of many other materials, and is comparable to those of layered cobalt oxides such as $NaCo_2O_4$ [3] and $Ca_3Co_4O_9$ [4]. Surprisingly, the Seebeck coefficient of $CaCo_2O_4$ shows no sign of saturation even at 380 K; it tends to increase with temperature still further beyond 380 K. The large value of the Seebeck coefficient suggests that $CaCo_2O_4$ is potentially a good candidate material for many practical high-temperature applications. The origin of the large Seebeck coefficient may be due to the residual spin entropy combined with holes doped into the triply degenerated Co^{3+} t_{2g} orbitals [5,33]. Koshibae et al. [5] have suggested the following expression for the Seebeck coefficient at the high-temperature limit for cobalt oxides having the Co^{3+} and Co^{4+} mixed valence state:

$$S = -\left(\frac{k_B}{e}\right)\ln\left(\frac{g_3}{g_4}\frac{x}{1-x}\right), \quad (2)$$

where g_i is the degeneracy of the Co^{i+} state (degrees of freedom for configurations of up or down spins in the degenerated 3d orbitals) and x is the concentration of the Co^{4+} ions. Based on the assumption that $g_3 = 1$, $g_4 = 6$ (low-spin states), and $x \sim 0.1$ for $CaCo_2O_4$, S is estimated to be ~344 μV/K at the high-temperature limit. This value is about twice that of the observed S (~147 μV/K) at 380 K. However, the observed S is still unsaturated even at 380 K; an increase is observed at higher temperatures. S is expected to approach the ideal value at the high-temperature limit. For ordinary transition-metal compounds, the high-temperature entropy in the d orbital is mostly released by various phase transitions with a decreasing temperature. However, in the case of cobalt oxides such as $NaCo_2O_4$ [3] and $Ca_3Co_4O_9$ [4], no transition occurs down to low temperatures. As a result of the restraint, there is a large residual spin entropy near room temperature, which couples with charges through mediation by strong electron correlation, due to the narrow d-orbital band, yielding a large thermoelectric power [5,34]. The present $CaCo_2O_4$ may also have the same mechanism, in essence, for generation of thermoelectric power as other cobalt oxides.

The temperature-dependent behavior of S above room temperature, i.e., unsaturated S, seems to be quite unique. For most cobalt oxides, S tends to saturate near 300 K [3,4,29,35–37]. In contrast, for $CaCo_2O_4$, S continues to increase monotonically as a function of temperature, even beyond 300 K. This behavior appears to be inconsistent with the thermal-activation-type temperature dependence of resistivity observed near 300 K. A reason for this phenomenon is not yet known. However, this phenomenon might have to be considered in terms of the relation between large residual spin entropy and strong electron correlation. Further precise studies are, therefore, necessary for a more detailed understanding of the electronic states in $CaCo_2O_4$. In particular, the measurement of the Seebeck coefficient at higher temperatures and carrier- or impurity-dopant synthesis experiments would be informative. Furthermore, the theoretical understanding of the physics of the cobalt oxides should be revisited.

The specific heat data were quantitatively analyzed using a well-known method. The raw data were plotted as C_p/T vs. T^2 as shown in Fig. 6. The following form was

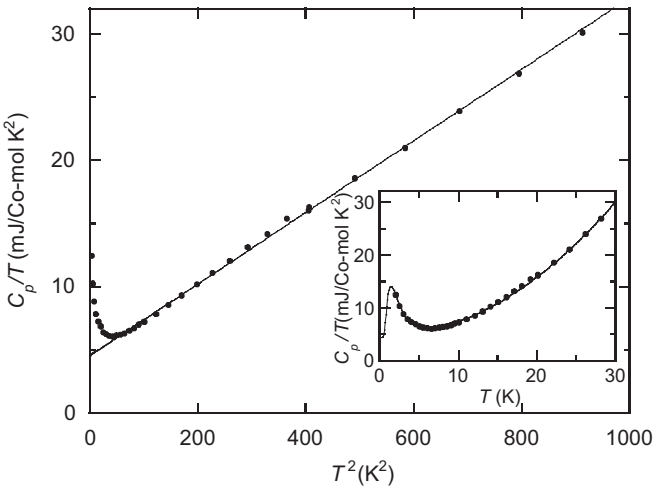

Fig. 6. Specific heat of $CaCo_2O_4$. Main panel: C_p/T vs. T^2 plot. Sommerfeld constant ($\gamma = 4.48(7)\,\mathrm{mJ/mol\,K^2}$) was obtained from extrapolation of the straight line. Inset: A result of the numerical analysis including correction of Schottky-type specific heat.

applied to fit the linear region using the least-squares method:

$$\frac{C_v}{T} = \gamma + \left(\frac{12\pi^4}{5}\right) r N_A k_B \left(\frac{1}{\theta_D^3}\right) T^2, \tag{3}$$

where N_A and r denote Avogadro's number and the number of atoms per formula unit, respectively. The two parameters, γ (electronic specific heat coefficient) and θ_D (Debye temperature), are material dependent. The analysis is valid in the low-temperature limit ($T \ll \theta_D$). The difference between C_p and C_v was assumed to be insignificant in the temperature range studied. As a result, the γ and θ_D values for $CaCo_2O_4$ were thus obtained as follows: $\gamma = 4.48(7)\,\mathrm{mJ/Co\,mol\,K^2}$ and $\theta_D = 621(1)\,\mathrm{K}$. The linear part of the data used for the analysis was $64\,\mathrm{K^2} \leqslant T^2 \leqslant 900\,\mathrm{K^2}$ ($8\,\mathrm{K} \leqslant T \leqslant 30\,\mathrm{K}$).

The compound is electrically insulating at low temperatures. The γ is, therefore, expected to be zero since the Fermi level would be in the band gap, however, this is not the case. Although the γ value of $CaCo_2O_4$ is smaller than those of metallic cobalt oxides [38–44], undoubtedly it is not zero. The non-zero γ indicates a finite density of states at E_F. The conduction band (or the in-gap state) is probably derived from the cobalt t_{2g} orbital; the Fermi level barely crosses the near edge of the band. The disorder in the crystal localizes carriers and forms isolated spins at low temperatures. This scenario is consistent with the other low-temperature properties as shown in Figs. 3–5. The origin of the carriers is probably due to the slight off-stoichiometry of the phase.

Enhancement of the specific heat was observed below 6 K. This behavior could be understood as a Shottky-type anomaly. The following equation was applied to fit the observed data using the least-square method

$$\frac{C_v}{T} = \beta_1 + \beta_3 T^2 + \left(\frac{c_0}{T}\right)\left(\frac{\Delta E}{k_B T}\right)^2 \frac{\exp(\Delta E/k_B T)}{(1+\exp(\Delta E/k_B T))^2}, \tag{4}$$

where ΔE is the difference between the discrete energy levels near the Fermi energy, and c_0 is a parameter with the dimensions of the specific heat. The two-level approximation model was assumed for the derivation of the equation [36]. The first and the second terms of the right side in Eq. (4) are electronic and lattice specific heat components, respectively. The third term, i.e., the correction term, is a component of the Schottky-type specific heat. The inset in Fig. 6 presents the calculated curve, which approximates well the observed data. The parameter values obtained are $\beta_1 = 4.32(8)\,\mathrm{mJ/Co\,mol\,K^2}$, $\beta_3 = 0.0285(2)\,\mathrm{mJ/Co\,mol\,K^4}$, $c_0 = 37(1)\,\mathrm{mJ/Co\,mol\,K}$, and $\Delta E = 0.41(2)\,\mathrm{meV}$. The temperature range used for the analysis was $2\,\mathrm{K} \leqslant T \leqslant 32\,\mathrm{K}$. The fairly good fit between the observed data and the calculated curve validates the analysis model for $CaCo_2O_4$. The origin of the discrete energy levels is probably associated with the dilute magnetic moments or carriers localized in the system.

4. Summary

We succeeded in synthesizing the $CaFe_2O_4$-type calcium cobalt oxide $CaCo_2O_4$ for the first time under high-temperature and high-pressure conditions. The local structure and, the magnetic and electrical properties were studied in detail. The calcium cobaltite $CaCo_2O_4$ was found to be a lightly hole-doped system having an almost fully filled cobalt t_{2g}-orbital band with a small localized density of states. The observed 3-D (or 2-D)-like transport properties suggest that the 1-D anisotropy expected in the $CaFe_2O_4$-type structure is weakened by an inter-chain orbital overlap in $CaCo_2O_4$. It was found that $CaCo_2O_4$ exhibits large thermoelectric power, possibly produced by coupling of residual spin entropy and charges mediated by electron correlation. Anomalous behavior in the temperature dependence of the Seebeck coefficients was also found. However, a conclusive interpretation of the data concerned with the thermally excited states could not be presented in this paper. This matter is, thereby, still an open question. Further studies using high-quality single crystals would help to clarify and develop an understanding of the physical properties and correlated electron behavior of the present compound. Since intriguing properties due to substantial electron correlations are expected, further synthesis and measurement studies are in progress.

Acknowledgments

We wish to thank Dr. Taniguchi (NIMS) for a lot of helpful advice about the high-pressure experiments. This

research was supported in part by the Superconducting Materials Research Project from the Ministry of Education, Culture, Sports, Science and Technology of Japan, and by the Grants-in-Aid for Scientific Research from the Japan Society for the Promotion of Science (Grant no. 19560686), and by the Iketani Science and Technology Foundation, Tokyo, Japan (Grant no. 0191125-A). The author (M.S.) would like to thank NIMS for supporting this work.

References

[1] K. Takada, H. Sakurai, E. Takayama-Muromachi, F. Izumi, R.A. Dilanian, T. Sasaki, Nature 422 (2003) 53.
[2] D.J. Singh, Phys. Rev. B 68 (2003) 020503(R).
[3] I. Terasaki, Y. Sasago, K. Uchinokura, Phys. Rev. B 56 (1997) R12685.
[4] A.C. Masset, C. Michel, A. Maignan, M. Hervieu, O. Toulemonde, F. Studer, B. Raveau, J. Hejtmanek, Phys. Rev. B 62 (2000) 166.
[5] W. Koshibae, K. Tsutsui, S. Maekawa, Phys. Rev. B 62 (2000) 6869.
[6] P.M. Hill, H.S. Peiser, J.R. Rait, Acta Crystallogr. 9 (1956) 981.
[7] O. Muller, R. Roy, The Major Ternary Structural Families, Springer, New York, 1974, p. 55.
[8] J. Akimoto, H. Takei, J. Solid State Chem. 79 (1989) 212.
[9] A.F. Wells, Structural Inorganic Chemistry, fifth ed., Clarendon Press, Oxford, 1984, p. 600.
[10] S. Zouari, L. Ranno, A. Cheikh-Rouhou, M. Pernet, P. Strobel, J. Mater. Chem. 13 (2003) 951.
[11] C.D. Ling, J.J. Neumeier, D.N. Argyriou, J. Solid State Chem. 160 (2001) 167.
[12] K. Yamaura, Q. Huang, L. Zhang, K. Takada, Y. Baba, T. Nagai, Y. Matsui, K. Kosuda, E. Takayama-Muromachi, J. Am. Chem. Soc. 128 (2006) 9448.
[13] J. Darriet, A. Vidal, Bull. Soc. Fr. Miner. Crystallogr. 98 (1975) 374.
[14] V.N. Skrobot, Russ. J. Inorg. Chem. 24 (1989) 1209.
[15] K. Yamaura, Q. Qingzhen Huang, M. Moldovan, D.P. Young, A. Sato, Y. Baba, T. Nagai, Y. Matsui, E. Takayama-Muromachi, Chem. Mater. 17 (2005) 359.
[16] T. Irifune, K. Fujino, E. Ohtani, Nature 349 (1991) 409.
[17] S. Ito, K. Suzuki, M. Inagaki, S. Naka, Mater. Res. Bull. 15 (1980) 925.
[18] C. Michel, M. Hervieu, B. Raveau, S. Li, M. Greaney, S. Fine, J. Potenza, M. Greenblatt, Mater. Res. Bull. 26 (1991) 123.
[19] P.W. Anderson, The Theory of Superconductivity in the High-T_C Cuprate Superconductors, Princeton Series in Physics, Princeton University Press, Princeton, NJ, 1997.
[20] A.P. Mackenzie, Y. Maeno, Rev. Mod. Phys. 75 (2003) 657.
[21] Y. Tokura, N. Nagaosa, Science 288 (2000) 462.
[22] Y. Miyazaki, M. Onoda, T. Oku, M. Kikuchi, Y. Ishii, Y. Ono, Y. Morii, T. Kajitani, J. Phys. Soc. Jpn. 71 (2002) 491.
[23] F. Izumi, T. Ikeda, Sci. Forum 321–324 (2000) 198.
[24] R.D. Shannon, Acta Crystallogr 32 (1976) 751.
[25] N.F. Mott, E.A. Davis, Electronic Processes in Non-crystalline Materials, second ed., Clarendon Press, Oxford, 1979 (Chapter 2).
[26] N.F. Mott, Conduction in Non-crystalline Materials, Clarendon Press, Oxford, 1987 (Chapter 3).
[27] I.P. Zvyagin, in: M. Pollak, B. Shklovskii (Eds.), Hopping Transport in Solids, Elsevier, North-Holland, Amsterdam, 1991, p. 143.
[28] $\ln\{-\mathrm{d}(\ln\sigma)/\mathrm{d}(\ln T)\}$ vs. $\ln T$ plot was used for the analysis of the resistivity data; B. Raquet, M.N. Baibich, J.M. Broto, H. Rakoto, S. Lambert, A. Maignan, Phys. Rev. B 65 (2002) 104442.
[29] M. Sánchez-Andújar, D. Rinaldi, R. Caciuffo, J. Mira, J. Rivas, M.A. Señarís-Rodríguez, Solid State Sci. 8 (2006) 901.
[30] R.L. Petritz, Phys. Rev. 104 (1956) 1508.
[31] L.L. Kazmerski, W.B. Berry, C.W. Allen, J. Appl. Phys. 43 (1972) 3515.
[32] Z.H. Wang, H.H.S. Javadi, A. Ray, A.G. MacDiarmid, A.J. Epstein, Phys. Rev. B 42 (1990) 5411.
[33] Y. Wang, N.S. Rogado, R.J. Cava, N.P. Ong, Nature 423 (2003) 425.
[34] P.M. Chaikin, G. Beni, Phys. Rev. B 13 (1976) 647.
[35] Y. Miyazaki, K. Kubo, M. Akoshima, Y. Ono, Y. Koike, T. Kajitani, Jpn. J. Appl. Phys. 39 (2000) L531.
[36] F. Chen, K.L. Stokes, R. Funahashi, Appl. Phys. Lett. 81 (2002) 2379.
[37] T. Itoh, I. Terasaki, Jpn. J. Appl. Phys. 39 (2000) 6658.
[38] Y. Ando, N. Miyamoto, K. Segawa, T. Kawata, I. Terasaki, Phys. Rev. B 60 (1999) 10580.
[39] T. Motohashi, R. Ueda, E. Naujalis, T. Tojo, I. Terasaki, T. Atake, M. Karppinen, H. Yamauchi, Phys. Rev. B 67 (2003) 064406.
[40] H. Sakurai, N. Tsujii, E. Takayama-Muromachi, J. Phys. Soc. Jpn. 73 (2004) 2393.
[41] T. Yamamoto, K. Uchinokura, I. Tsukada, Phys. Rev. B 65 (2002) 184434.
[42] P. Limelette, V. Hardy, P. Auban-Senzier, D. Jérome, D. Flahaut, S. Hébert, R. Frésard, Ch. Simon, J. Noudem, A. Maignan, Phys. Rev. B 71 (2005) 233108.
[43] P. Limelette, S. Hebert, V. Hardy, R. Fresard, C. Simon, A. Maignan, Phys. Rev. Lett. 97 (2006) 046601.
[44] S. Balamurugan, K. Yamaura, A.B. Karki, D.P. Young, M. Arai, E. Takayama-Muromachi, Phys. Rev. B 74 (2006) 172406.